ISSN (Print) 1226-1750
ISSN (Online) 2233-6656
Journal of Magnetics 24(4), 650-656 (2019) https://doi.org/10.4283/JMAG.2019.24.4.650

Suppression of α-Fe_2O_3 Phase in $MgFe_2O_4$ Nanoparticles with High Magnetization by Controlling Annealing Process

Shanigaram Mallesh and Ki Hyeon Kim*

Department of Physics, Yeungnam University, Gyeongsan 38541, Republic of Korea

(Received 4 September 2019, Received in final form 31 October 2019, Accepted 5 December 2019)

We report the phase stability, microstructure and magnetic properties of $MgFe_2O_4$ nanoparticles under different annealing conditions. Magnetic properties of $MgFe_2O_4$ are strongly influenced by the crystal structure and morphology, which in turn, depend on annealing conditions. The as-prepared and samples annealed at 1200 °C show a pure spinel phase. Whereas the samples annealed and quenched at 600 °C-1000 °C exhibit the spinel phase along with a small fraction of the secondary phase of α-Fe_2O_3, which causes deterioration of magnetic properties. On the other hand, samples annealed at 600 °C-1000 °C under Argon atmosphere display superior magnetic properties (M = 44-56 emu/g at room temperature) due to the presence of pure spinel phase. Interestingly, the sample quenched at 1200 °C exhibits large saturation magnetization, M_S = 63 emu/g at 5 K which is arising from the optimum cationic distribution (δ = 0.77) grown at elevated temperature is retained in the rapid cooling process.

Keywords : nanoparticles, thermal stability, microstructure, soft-ferrite, saturation magnetization, superparamagnetic

1. Introduction

The spinel ferrite nanoparticles (NPs) have gained remarkable interest due to their high surface to volume ratio, large saturation magnetization, low hysteresis loss, low toxicity, biocompatibility, electrical and optical properties [1, 2]. Among the various cubic spinels, $MgFe_2O_4$ (MgFO) has been widely explored owing to its intriguing optical, catalytic and soft magnetic properties for various potential applications, such as lithium-ion batteries, water splitting, photocatalysts, sensors and in biological applications [3-7].

Recently, several authors studied the structural and magnetic properties of MgFO NPs synthesized by different methods such as solid-state reaction, high-temperature thermal decomposition [8], solvothermal [9], mechano-chemical rout [10], ultrasonic wave assisted ball milling [11] and sol-gel process [6]. These reports advocate that the morphology and magnetic properties of the NPs can be controlled by the precursors and variation of synthesis conditions. However, the as-prepared NPs possess strain and surface disorder, which results inferior magnetic properties. To further improve the magnetic properties of MgFO NPs by decreasing the strain and surface disorder therefore, the NPs have to be heat-treated at moderate temperatures (600 °C-1000 °C). Unfortunately, the spinel ferrite (few spinels like $MOFe_2O_4$, M = Fe, Mn & Mg) phase is unstable in this temperature range, therefore they exhibit secondary phases such as α-Fe_2O_3, α-Mn_2O_3 and MgO along with spinel structure [12-15], which causes a decrease in magnetic properties. On the other hand, a pure ferrite phase with large saturation magnetization is required for the above mentioned applications. Though, the ZnO coating on ferrite NPs (ferrite@ZnO core-shell structures) results in a stable spinel phase (600 °C) [16, 17], however, the magnetization is decreased because of the annealing temperature which leads to the formation of Zn-rich ferrite phase at the interface of MgFO@ZnO core-shell structures [17]. Similarly, Feng *et al*. also observed the stable ferrite phase in PVA assisted $MgFe_2O_4$ NPs with excess Mg concentrations. But, they exhibit weak magnetization when annealed in the temperature range from 500 °C-700 °C [18]. Therefore, a systematic study is essential to stabilize the spinel phase at intermediate temperatures (500 °C-1000 °C) to improve the soft magnetic properties of $MgFe_2O_4$ NPs.

Herein, we report the phase stability and magnetic properties of the MgFO NPs prepared by the sol-gel process.

*Corresponding author: Tel: +82-53-810-2334
Fax: +82-53-810-4616, e-mail: kee1@ynu.ac.kr

The as-prepared samples were processed under different annealing conditions in the temperature range from 350 °C to 1200 °C to develop the soft magnetic properties by suppressing the secondary phases.

2. Experimental Details

The MgFO NPs were prepared by the sol-gel process according to the previous report on MnZn ferrite NPs [13]. The stoichiometric ratio of the $Mg(NO_3)_2{\cdot}6H_2O$ and $Fe(NO_3)_3{\cdot}9H_2O$ precursors were dissolved in 30 ml of ethylene glycol and thereafter glycerol was slowly added to stabilize the solution. The homogeneous solution was obtained after vigorous magnetic stirring at 75 °C, then the solution is cooled to room temperature. After cooling the solution to room temperature it was again dissolved in 75 ml of 2-proponal, followed by a dropwise addition of 37 ml Try ethyl amine (acts as a catalyst) with continuous stirring for 10 minutes. Finally, the solution turned into a thick brown color gel which was heated at 150 ºC to obtain the as-prepared NPs. The as-prepared (*AP*) NPs were heat-treated in two different conditions followed as (i) samples annealed & quenched (Q) in liquid nitrogen and (ii) annealed in Argon (Ar) atmosphere in the temperature range from 350 ºC-1200 ºC to improve the magnetic properties by controlling secondary phases. Subsequently, the results were compared with the air annealed and furnace cooled (FC) samples [17]. The X-ray diffraction (XRD) data were obtained by using PANalytical (X'pert PRO) with CuKα (λ = 1.54059 Å) radiation. The structure and crystallographic phase formations of the differently heat-treated samples were analyzed by Rietveld refinement using GSAS software. Raman spectrometer (Jobin-Yvon LabRAM HR800UV) with 633 nm emission line of He-Ne laser was used to study the vibrational properties of the samples. The evolution of morphology with heat-treatment has been investigated by field emission scanning electron microscopy (FESEM) using Inspect F50. The magnetic measurements were carried out by Microsense EV9 vibrating sample magnetometer (VSM) at room temperature (RT). The temperature-dependent magnetization in zero-field-cooled (ZFC) & field-cooled (FC) conditions and isothermal magnetization (M-H curves) at different temperatures were measured by using Quantum Design SQUID VSM.

3. Results and Discussions

Fig. 1(a) shows the XRD patterns of the quenched samples exhibiting the cubic spinel phase along with a small amount of secondary phase (α-Fe_2O_3) in the temperature range from 600 °C-1000 °C, which is similar to the furnace cooled samples. However, the observed weight fraction of the secondary phase is significantly reduced compared to that of furnace cooled samples [17]. Further, a pure stable ferrite phase reappears in 1200 °C Q sample with improved crystallinity. On the other hand, samples annealed (600 °C-1200 °C) in Ar atmosphere exhibit a single-phase spinel structure with improved crystallinity as shown in Fig. 1(b). The previous reports on the phase stability of ferrites demonstrated that the oxidation takes place in samples when annealed in the temperature range from 600 °C to 1000 °C in air and oxygen due to the difference in oxygen partial pressure [13, 17]. Whereas, the oxidation process is suppressed in samples when annealed in inert (Ar) atmosphere. Therefore, the oxidation can be controlled by the cooling process and annealing environments. The average crystallite size (estimated using Scherrer formula) is 12 nm for *AP* NPs, which increases with the increment of annealing temperature (85 nm for 1000 °C Ar) and approaches bulk value for the sample annealed at 1200 °C in Ar atmosphere (see Table 1). Fig. 1(e) shows the XRD pattern with Rietveld refinement

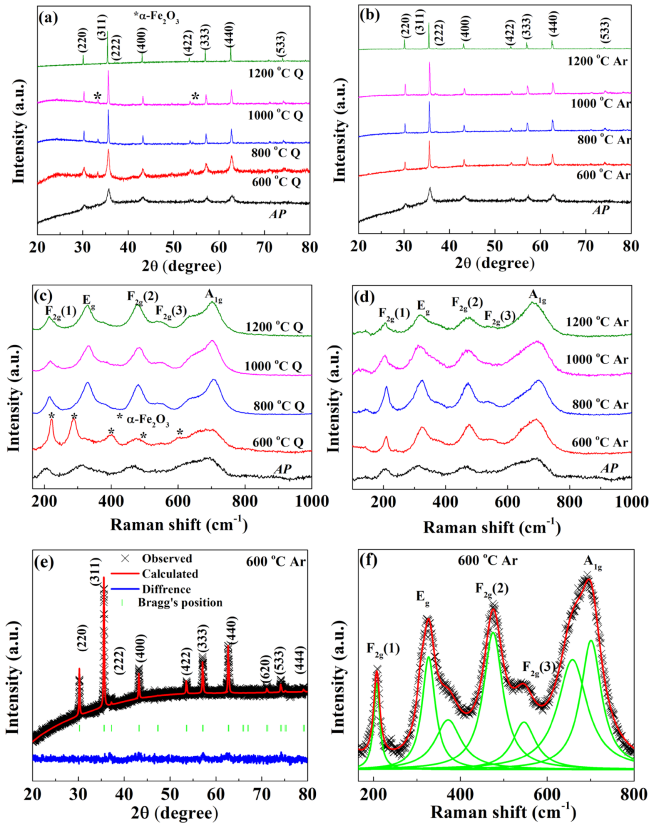

Fig. 1. (Color online) XRD patterns and Raman spectra of $MgFe_2O_4$ (a, c) quenched & (b, d) Argon annealed samples respectively. (e) Rietveld refinement of XRD pattern and (f) Raman spectra along with modes for 600 °C Ar sample.

Table 1. The structural parameters and vibrational mode A_{1g} for $MgFe_2O_4$ as-prepared and differently annealed samples. Where t and 'a' represent crystallite size and lattice parameter.

Samples	t (nm)	a (Å)	A_1g (cm^{-1})	
AP	11	8.3830(8)	632	696
600 °C Q	15.5	8.3919(5)	663	708
800 °C Q	50	8.3928(2)	660	709
1000 °C Q	93	8.3936(2)	651	703
1200 °C Q	bulk	8.3967(6)	650	698
600 °C Ar	57.6	8.3918(3)	658	700
800 °C Ar	77	8.3933(2)	649	705
1000 °C Ar	85	8.3991(1)	656	703
1200 °C Ar	bulk	8.3998(4)	656	694

analyses at 600 °C under Ar. The lattice parameters obtained from Rietveld refinement are summarized in Table 1. It is observed that the lattice parameter 8.3830(3) Å for *AP* NPs increases to 8.3998(4) for 1200 °C Ar annealed sample (Table 1). Similar behavior is also observed in quenched samples. These observed results are in agreement with the earlier report [19]. The relative distribution of Mg^{2+} and Fe^{3+} cations over tetrahedral and octahedral sites changes with annealing temperature leads to an increase of lattice parameter.

Fig. 1(c, d) demonstrates the Raman spectra of MgFO quenched and Argon annealed samples recorded at room temperature in the frequency range from 100-1000 cm^{-1}. The Raman modes corresponding to the pure spinel phase observed in all samples except 600 °C quenched sample, which exhibits a cubic spinel phase along with a small amount of secondary phase (α-Fe_2O_3). Further, the Raman spectra were fitted using Lorentzian to obtain the number of Raman modes and their natural frequencies as shown in Fig. 1(f) for a typical 600 ºC Ar sample. The presence of five Raman active modes is the characteristic vibrational modes of the spinel phase. The additional Raman mode around 630-660 cm^{-1} is observed for all the samples which is due to the order-disorder effect of two metal (Mg^{2+} & Fe^{3+}) ions at tetrahedral and octahedral sites, respectively [20]. This order-disorder effect might change significantly with different annealing conditions. The frequency positions of A_{1g} mode obtained from the fitting are shown in Table 1. The frequency position of Raman modes A_{1g} (694-709 cm^{-1}), $3F_g$ (536-548 cm^{-1}, 460-483 cm^{-1}, 204-219 cm^{-1}) and E_g (315-329 cm^{-1}) are observed for all samples corresponding to the ferrites phase.

Fig. 2 shows the FESEM images of the *AP* and differently heat-treated MgFO samples, respectively. The morphology of the *AP* NPs agglomerated and exhibit hazy

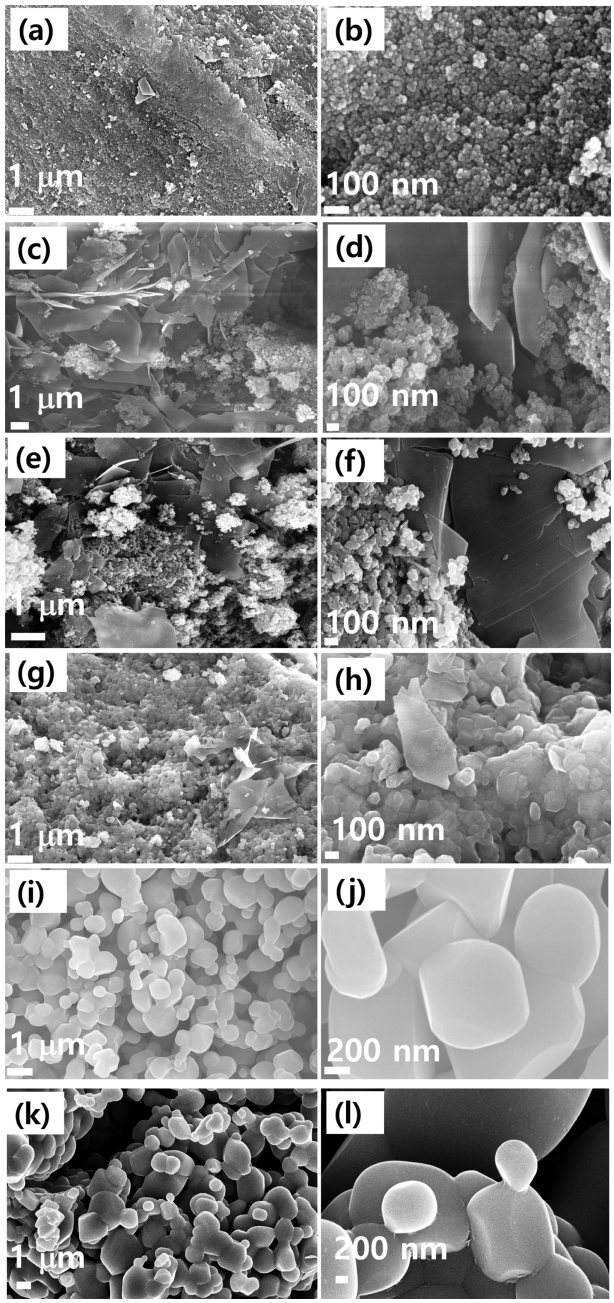

Fig. 2. FESEM images of $MgFe_2O_4$ (a, b) *AP* and samples annealed at (c, d) 600 °C in air, (e, f) 600 °C Ar, (g, h) 1000 °C Ar, (i, j) 1200 °C in air, and (k, l) 1200 °C Q.

spherical shape with the average particle size of ~20 nm as shown in Fig. 2(a, b). On annealing at 600 °C in air, the morphology of the aggregated NPs was grown into flakes-like structure (about few microns in size) along with the NPs as shown in Fig. 2(c, d). Fig. 2(e, f) illustrates the similar morphology of flakes-like structure with the combination of NPs observed for the sample annealed at 600 °C Ar. The morphology of flakes-like structure and the combination of NPs are retained in the sample annealed

at 1000 °C Ar as shown in Fig. 2(g, h). However, the agglomeration of NPs increases with the average particle size of ~100 nm for 1000 °C Ar annealed sample. Further, increasing the annealing temperature (1200 °C), the NPs aggregated and grown into polyhedral-like morphology with heterogeneous grain size distributions from 0.2 μm to 1 μm for 1200 °C annealed and furnace cooled sample as revealed in the Fig. 2(i, j). A similar morphology is observed for 1200 °C Q sample with the average grain size ranges from 1 μm to 3 μm as depicted in Fig. 2(k, l). The detailed FESEM study reveals that the annealing temperature and processing conditions show a significant effect on the morphologies of the samples.

Fig. 3(a, b) shows the isothermal M-H curves measured at RT for quenched and Argon annealed samples. The magnetization of the *AP* and samples annealed at low temperatures (< 1000 °C) is not saturated within the applied field (20 kOe). Whereas, the magnetization of samples annealed at 1200 °C is saturated at low field region (< 5 kOe). This behavior is due to the decreased surface disorder in samples with an increase of annealing temperature. The magnetization (M) and coercivity (H_C) obtained from M-H curves are plotted as a function of annealing temperature in comparison with the FC samples as shown in Fig. 3(c, d). The samples annealed in the temperature range from 600 °C-1000 °C Q show weak magnetic moment (18-31 emu/g) similar to the FC samples due to the presence of the impurity phase (α-Fe_2O_3). Further 1200 °C Q sample exhibit large saturation magnetization (43 emu/g) due to the presence of pure spinel structure with improved crystallinity. The observed results are in good agreement with earlier reports on quenched samples [14, 19]. On the other hand, the value of M is 48 emu/g for 600 °C Ar sample increases to 56 emu/g for 1000 °C Ar sample, which is highest at RT observed so far for $MgFe_2O_4$ samples synthesized by sol-gel process. The high magnetization in Ar annealed samples is attributed to the increase in crystallite (particles) size and the morphology (large surface to volume ratio & surface effects). Further, the value of M is found to be decreased to 37 emu/g for 1200 °C Ar annealed sample. This could be due to the redistribution of cations between tetrahedral and octahedral sites with an increase of annealing temperature and a decrease of surface effects [21-23]. The maximum value of H_C is ~75 Oe for 800 °C FC and Q samples, which is attributed to the presence of spinel and secondary phases. Further, H_C decreases to below 30 Oe as the annealing temperature reaches 1200 °C, this could be due to the increase of size and decrease of surface effects. On the other hand, the large value of H_C (~131 Oe) obtained for the 600 °C Ar sample due to the finite size effects [Fig. 3(d)]. These observations corroborate well with microstructural data and suggest that the annealing processes play an important role in enhancing the magnetic properties by controlling the impurity phases.

Fig. 4 Depicts the temperature-dependent magnetization measured under ZFC/FC protocols in the presence of 100 Oe magnetic field for *AP* and 1200 °C Q samples. The

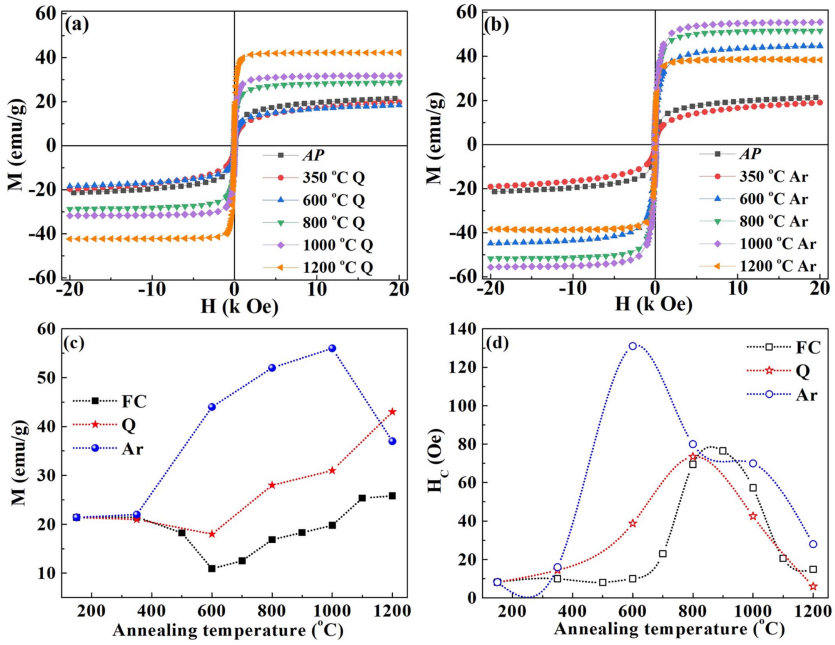

Fig. 3. (Color online) Isothermal M-H curves of $MgFe_2O_4$ (a) quenched and (b) Ar annealed samples. (c, d) The magnetization and coercivity as a function of annealing temperature for differently heat-treated $MgFe_2O_4$ samples.

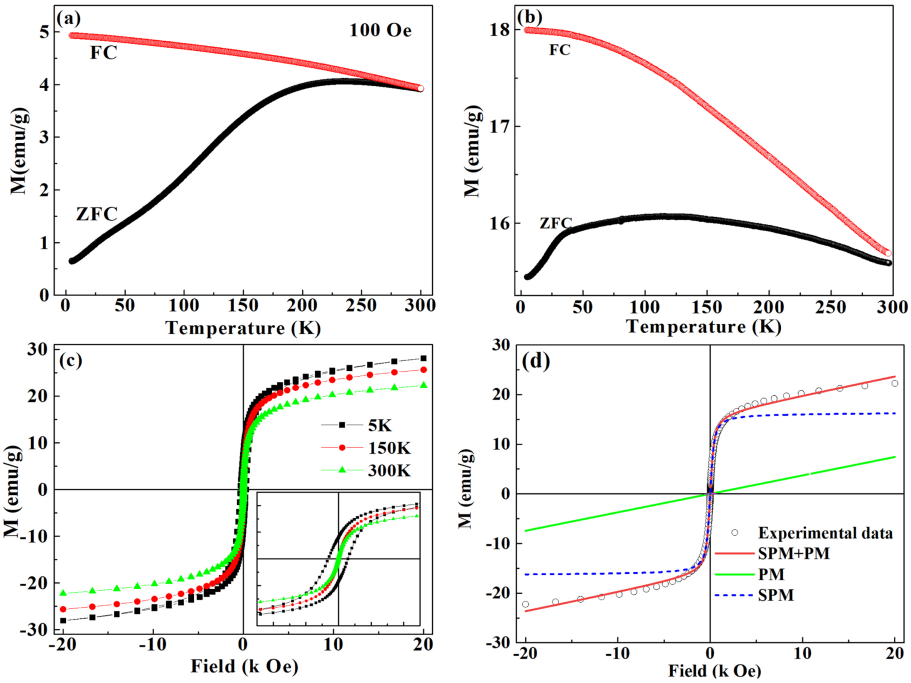

Fig. 4. (Color online) ZFC-FC magnetization of $MgFe_2O_4$ (a) *AP* and (b) 1200 °C Q samples. (c) M-H curves measured at different temperatures and (d) Langevin fit to the RT M-H curve along with SPM+PM parts for $MgFe_2O_4$ *AP* sample.

ZFC magnetization of *AP* sample exhibits a broad temperature maximum (T_{max}) around 230 K and the separation between the ZFC/FC curves (irreversible temperature, T_{irr}) is observed near 300 K. The average blocking temperature (T_B = 125K) can be obtained from a relation with ZFC maximum, $T_{max} = \beta <T_B>$ where the β values can be varied from 1.5 to 2. The existence of T_{max} and T_{irr} resemble the superparamagnetic (SPM)-like behavior in *AP* NPs. The SPM behavior in MgFO NPs also observed in earlier reports [10, 21-23]. On the other hand, ZFC and FC magnetizations of the 1200 °C Q sample are different compared to that of *AP* sample. In addition, FC/ZFC data at above RT exhibit irreversible magnetization behavior indicating a magnetic disorder in the bulk composition too. This behavior can be speculated as due to the ferrimagnetic nature of the system [1, 24]. Fig. 4(c) demonstrates the M-H curves measured at three different temperatures for MgFO *AP* sample. The magnetization of *AP* NPs exhibit symmetric hysteresis with large H_C (~ 302 Oe) at 5 K and negligible H_C (unhysteretic) at 300 K, which indicates the SPM-like behavior. Fig. 4(d) displays the RT M-H curve of the *AP* MgFO sample is fitted with the following modified Langevin equation [16];

$$M = M_S\left[\coth\left(\frac{\mu H}{k_B T}\right) - \left(\frac{k_B T}{\mu H}\right)\right] + \chi_f H \qquad (1)$$

where, the M_S is the saturation magnetization, μ is the magnetic moment of a single particle, k_B is Boltzmann constant and χ_f is the high field magnetic susceptibility of the linear paramagnetic term. The values of M_S = 16.2 emu/g, $\chi_f = 3.7 \times 10^{-4}$ em/g-Oe and μ ~ 9728 μ_B, respectively are obtained from the fitting. The large value of the magnetic moment reveals that each *AP* NPs contain large no of spins which is known as superspin.

Fig. 5(a) shows the magnetization of 600 °C Ar sample which is increased compared to that of *AP* sample, which shows clear hysteresis at all the temperatures indicating the development of ferrimagnetic order due to the increase of crystallite (particle) size. Further, the samples annealed at 1200 °C (Q & Ar) exhibit saturation magnetization within the applied field of 3 kOe which indicates the bulk properties [Fig. 5(b, c)]. Therefore, the law of approach to saturation (LAS) is used to obtain the saturation magnetization. The high field magnetization is fitted with the LAS for cubic systems as shown in Fig. 5(d) for 1200 °C Q sample [25];

$$M = M_S\left(1 - \frac{a}{H} - \frac{b}{H^2}\right) + \chi_f H \qquad (2)$$

where, χ_f is the high-field susceptibility and '*a*' is strain due to the defects in the system. The constant *b* is related to the anisotropy as $b = 8K_1^2/105\mu_0^2 M_S^2$ for randomly oriented cubic systems. The parameters obtained from the fitting are summarized in Table 2. The saturation magnetization and the anisotropy constant are found to be decreased with the increase of temperature due to the thermal

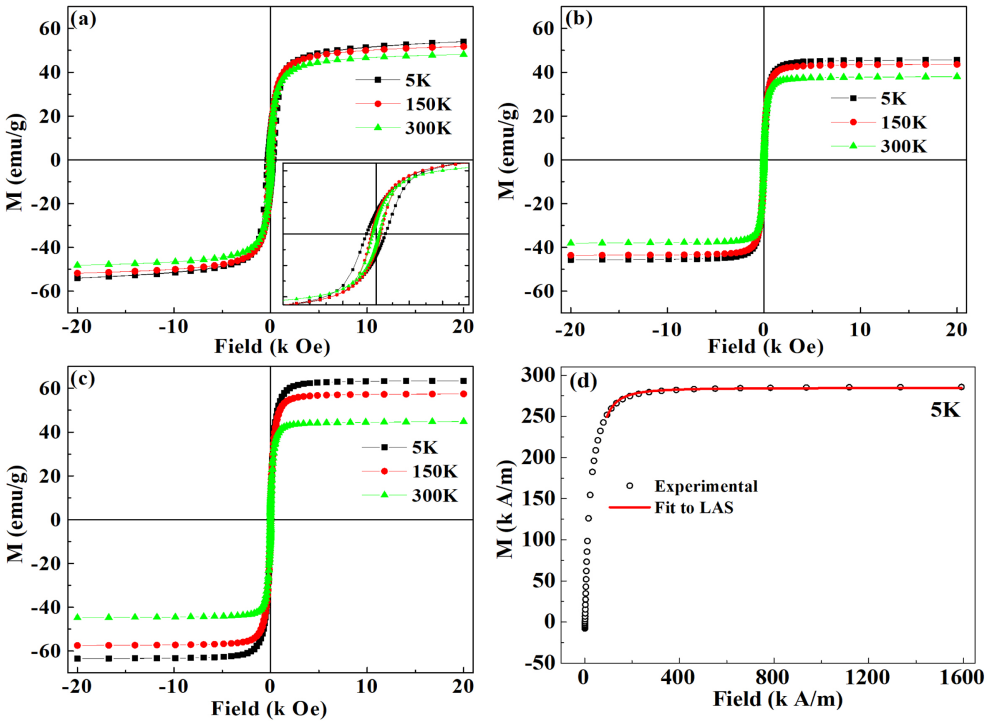

Fig. 5. (Color online) M-H curves measured at three different temperatures for (a) 600 °C Ar, (b) 1200 °C Ar and (c) 1200 °C Q samples. (d) LAS fit to the 1200 °C Q sample measured at 5 K.

Table 2. The saturation magnetization (M_S), Anisotropy constant (K_1) obtained from the fitting to the LAS for differently annealed $MgFe_2O_4$ samples.

Samples	Temperature (K)	H_C (Oe)	M_S (emu/g)	K_1 (10^5erg/cc)	χ_f (emu/g-Oe)
600 °C Ar	5	288	50	0.58135	1.8×10^{-2}
	150	130	47	0.48242	1.4×10^{-2}
	300	99	43	0.40375	1.4×10^{-2}
1200 °C Ar	5	20	45.4	0.31624	
	150	8.5	43.4	0.25828	
	300	0.9	37.6	0.18900	
1200 °C Q	5	15	63	0.41465	
	150	22	55.6	0.33696	
	300	26.5	43.4	0.23118	

agitations. The high value of $M_S = 50$ emu/g is observed at 5 K for 600 °C Ar sample which is enhanced about 50 % compared to it's bulk [M_S (bulk) = 33.4 emu/g] counterpart [22, 23]. Thus, the observed value of M_S is 45 emu/g for 1200 °C Ar sample, however, the enhanced value of M_S is 63 emu/g at 5 K for 1200 °C Q sample. To the best of our knowledge, this high M_S is not observed for bulk MgFO samples. Koferstein *et al.* observed the $M_S = 50$ emu/g at 10 K for the sample annealed at 900 °C, further M_S is decreased to 32-36 emu/g when annealed in the temperatures 1450 °C-1600 °C [21]. Sumangala *et al.* reported the $M_S = 56$ emu/g at 5 K in MgFO NPs sample synthesized by sol-gel combustion method and quenched from 800 °C [14]. Thanh *et al.* obtained $M_S = 58.82$ emu/g in 40.9 nm MgFO sample synthesized by combustion method and quenched from 1000 °C [19]. The enhancement of magnetization can be attributed to the change in cationic distribution in samples. The general expression for cations distribution is $(Mg^{2+}_{1-\delta}Fe^{3+}_{\delta})_{tet}[Mg^{3+}_{\delta}Fe^{3+}_{2-\delta}]_{oct}$, for MgFO, where δ is the inversion parameter (δ=0 for normal spinels & δ=1 for inverse spinels). The bulk MgFO exhibits a nearly inverse (δ=0.9) spinel structure [22, 23]. The magnetic moment per formula unit is defined as $n_B = \mu_{[B]} - \mu_{(A)} = 1.1 \times 5\ \mu_B - 0.9 \times 5\ \mu_B = 1\ \mu_B$, which is calculated by assuming collinear spin structure [10, 22, 23]. Therefore, the ferrimagnetic ordering of the Fe^{3+} (5 μ_B) ions at tetrahedral and octahedral sites results in the net magnetic moment (since Mg^{2+} is nonmagnetic, 0 μ_B). Besides this, the n_B is evaluated experimentally by using a relation $n_B = \frac{Mol.wt \times M_s}{5585}$ [25], where M_S is the saturation magnetization (emu/g) measured at 5 K and the inversion parameter is obtained using n_B values. The obtained values of n_B and are 1.80 μ_B, 1.62 μ_B & 2.26 μ_B and 0.82, 0.84 & 0.77, respectively for 600 °C Ar, 1200 °C Ar and 1200 °C Q samples. The increase of magnetic moment in NPs is due to the large surface to volume ratio, surface effects

and the cationic disorder (i.e. $\delta < 0.9$). Whereas, the unusual increase of magnetic moment in case of 1200 ºC Q samples is solely due to the presence of cationic disorder ($\delta = 0.77$). The structural characterization studies (crystallite/particle size) and saturation of magnetization at low fields indicate the bulk properties of 1200 ºC Q sample (absence of surface effects). Therefore, during heat-treatment the optimum cation distribution grown at elevated temperature is retained in quenched samples leads to improved soft magnetic properties.

4. Conclusions

The effect of annealing conditions on stability of the spinel phase, microstructure and magnetic properties of MgFO *AP* NPs have been investigated. The temperature and field-dependent magnetization investigations of the *AP* sample resembled the SPM-like behavior. The quenched samples exhibit weak magnetic characters due to the presence of the impurity phase α-Fe_2O_3 when particles are subjected to heat-treated 600 °C ≤ T ≤ 1000 °C. On the other hand, samples annealed (600 °C-1200 °C) under Ar atmosphere exhibited single-phase ferrite with superior magnetic properties. The soft magnetic properties were enhanced in 1200 °C Q sample attributed to the presence of cationic disorder in bulk samples.

Acknowledgment

This research was supported by Nano·Material Technology Development Program through the National Research Foundation of Korea (NRF) funded by the Ministry of Science, ICT and Future Planning (No. 2016M3A7B4900267).

References

[1] A. Goldman, Modern ferrite technology, Springer, Pittsburg (2006).
[2] A. Tomitaka, M. Jeun, S. Bae, and Y. Takemura, J. Magn. **16**, 164 (2011).
[3] Y. Pan, Y. Zhang, X. Wei, C. Yuan, J. Yin, D. Cao, and G. Wang, Electrochim. Acta **109**, 89 (2013).
[4] R. Dillert, D. H. Taffa, M. Wark, T. Bredow, and D. W. Bahnemann, APL Mater. **3**, 104001 (2015).
[5] K. Kirchberg, A. Becker, A. Bloesser, T. Weller, J. Timm, C. Suchomski, and R. Marschall, J. Phys. Chem. C **121**, 27126 (2017).
[6] Y.-L. Liu, Z.-M. Liu, Y. Yang, H.-F. Yang, G.-L. Shen, and R.-Q Yu, Sensor Actuat. B **107**, 600 (2005).
[7] V. M. Khot, A. B. Salunkhe, N. D. Thorat, R. S. Ningthoujam, and S. H. Pawar, Dalton Trans. **42,** 1249 (2013).
[8] S. W. Hyun, H. J. Kim, C. S. Park, K.-S. Kang, and C. S. Kim, IEEE Trans. Magn. **45**, 2551 (2009).
[9] L. Zheng, K. Fang, M. Zhang, Z. Nan, L. Zhao, D. Zhou, M. Zhu, and W. Li, RSC Adv. **8**, 39177 (2018).
[10] B. Antic, N. Jovic, M. B. Pavlovic, A. Kremenovic, D. Manojlovic, M. V. Vasic, and A. S. Nikolic, J. Appl. Phys. **107**, 043525 (2010).
[11] D. Chen, D. Li, Y. Zhang, and Z. Kang, Ultrason. Sonochem. **20**, 1337 (2013).
[12] A. Jafari, S. F. Shayesteh, M. Salouti, and K. Boustani, J. Magn. Magn. Mater. **379**, 305 (2015).
[13] S. Mallesh and V. Srinivas, J. Magn. Magn. Mater. **475**, 290 (2019).
[14] T. P. Sumangala, C. Mahender, B. N. Sahu, N. Venkataramani, and S. Prasad, Physica B **448**, 312 (2014).
[15] A. C. Druc, A. M. Dumitrescu, A. I. Borhan, V. Nica, A. R. Iordan, and M. N. Palamaru, Cent. Eur. J. Chem. **11**, 1330 (2013).
[16] S. Mallesh, A. Sunny, M. Vasundhara, and V. Srinivas, J. Magn. Magn. Mater. **418**, 112 (2016).
[17] S. Mallesh, D. Prabu, and V. Srinivas, AIP Adv. **7**, 056103 (2017).
[18] Y. Feng, S. Li, Y. Zheng, Z. Yi, Y. He, and Y. Xu, J. Alloys Compd. **699**, 521 (2017).
[19] N. K. Thanh, T. T. Loan, N. P. Duong, L. N Anh, D. T. T. Nguyet, N. H. Nam, S. Soontaranon, W. Klysubun, and T. D. Hien, Phys. Status Solidi A **215**, 1700397 (2018).
[20] Z. Wang, P. Lazor, S. K. Saxena, and H.-O. Neill, Mater. Res. Bull. **37**, 1589 (2002).
[21] R. Koferstein, T. Walther, D. Hesse, and S. G. Ebbinghaus, J. Mater. Sci. **48**, 6509 (2013).
[22] V. Sepelak, D. Baabe, D. Mienert, F. J. Litterst, and K. D. Becker, Scr. Mater. **48**, 961 (2003).
[23] V. Sepelak, A. Feldhoff, P. Heitjans, F. Krumeich, D. Menzel, F. J. Litterst, I. Bergmann, and K. D. Becker, Chem. Mater. **18**, 3057 (2006).
[24] P. Holec, J. Plocek, D. Niznansky, and J. P. Vejpravova, J. Sol-Gel Sci. Technol. **51**, 301 (2009).
[25] L. Neel, J. Phys. Rad. **9**, 184 (1948).